



HAL
open science

Influence of the variability of soil profile properties on weak and strong seismic response

Stefania Gobbi, Luca Lenti, Maria Paola Santisi D'avila, Jean-François Semblat, Philippe Reiffsteck

► **To cite this version:**

Stefania Gobbi, Luca Lenti, Maria Paola Santisi D'avila, Jean-François Semblat, Philippe Reiffsteck. Influence of the variability of soil profile properties on weak and strong seismic response. *Soil Dynamics and Earthquake Engineering*, 2020, 135, pp.106200. 10.1016/j.soildyn.2020.106200 . hal-03238056

HAL Id: hal-03238056

<https://hal.science/hal-03238056>

Submitted on 26 May 2021

HAL is a multi-disciplinary open access archive for the deposit and dissemination of scientific research documents, whether they are published or not. The documents may come from teaching and research institutions in France or abroad, or from public or private research centers.

L'archive ouverte pluridisciplinaire **HAL**, est destinée au dépôt et à la diffusion de documents scientifiques de niveau recherche, publiés ou non, émanant des établissements d'enseignement et de recherche français ou étrangers, des laboratoires publics ou privés.

1 **Influence of the variability of soil profile properties on weak and strong seismic response**

2

3 Stefania Gobbi^{a,*}, Luca Lenti^{a,d}, Maria Paola Santisi d'Avila^b, Jean-François Semblat^c,

4 Philippe Reiffsteck^a

5

6 ^a Université Gustave Eiffel, IFSTTAR (GERS/SRO), Marne la Vallée, France

7 ^b Polytech'Lab, EA UNS 7498, Université Côte d'Azur, Sophia Antipolis, France

8 ^c IMSIA (UMR9219), CNRS, EDF, CEA, ENSTA Paris, Institut Polytechnique de Paris,

9 France

10 ^c Cerema, Equipe-Projet MOUVGS, Sophia Antipolis, France

11

12

13 Corresponding author:

14 Stefania Gobbi

15 Université Gustave Eiffel, IFSTTAR (GERS/SRO)

16 14-20 Boulevard Newton - 77420 Champs sur Marne - France

17 Email: stefania.gobbi@ifsttar.fr

18

19 **ABSTRACT**

20 Characterizing the potential effect of local site conditions on the amplification of ground
21 motions is a critical aspect of seismic hazard and risk assessment. The aim of this study is to
22 investigate the reliability and the limit of using the average shear wave velocity in the upper
23 30m of the soil profile $v_{s,30}$, as single proxy, to characterize seismic site effects for weak and
24 strong events.

25 To this regard, a dataset of 300 one-dimensional soil profiles with a given $v_{s,30}$ are generated
26 through a Monte Carlo approach. Their seismic responses are computed for a set of 40 real
27 accelerograms, with different seismic features. The vertical propagation from the bottom of
28 the generated columns is modeled using a finite element spatial discretization, accounting for
29 both linear and nonlinear soil behavior.

30 The site dominant frequency f_0 and the shear wave velocity gradient in the profile B_{30} are
31 proposed as proxies to characterize seismic site effects and the variability of the response
32 spectra for the numerical signals, at the free surface of the set of columns, is discussed.
33 Correlations between site-specific amplification factors deduced using the numerical response
34 spectra and the proposed site proxies are analyzed for different sub-ranges of periods. The
35 obtained amplification factors are then compared to those proposed by different international
36 and national design codes.

37 The results, obtained under assumption of linear and nonlinear behavior of soil, emphasize the
38 need to introduce complementary site parameters proxies, in addition to $v_{s,30}$, to characterize
39 the expected site effects in design response spectra.

40

41 **Keywords:** Geotechnical properties, site effects, variability, average shear wave velocity,
42 impedance contrast, response spectrum, Eurocode 8.

43

44 **1. Introduction**

45 Recent and past earthquakes, such as 1985 Mexico City, 1989 Loma Prieta, 1994
46 Northridge, 1995 Kobe events, among others, underline the need to characterize the effect
47 of the local soil conditions on seismic site response prediction. It has been widely recognized
48 that the seismic site effects are generally related to the stratigraphy, the surface topography,
49 the impedance contrast and the rheology of the soils involved during the propagation of
50 seismic waves [1].

51 Current seismic design codes consider the seismic site effects through a ground type
52 classification solely based on the average shear velocity in the upper 30m of the soil profile
53 $v_{s,30}$ proposed by Borchardt [2], neglecting the depth of the bedrock and the property of the
54 soil below 30m. Nevertheless, it has been recognized that $v_{s,30}$ is a useful parameter to capture
55 some features of the local site amplification effects [3–7].

56 However, several researches [8–15] show that $v_{s,30}$ cannot be used as the single-site proxy to
57 discriminate soils in terms of seismic amplification over the whole frequency range of
58 interest. To this regard, Steidl [16] and Park and Hashash [8] recommended the introduction
59 of a depth-to-bedrock parameter since they found that the provisions based on $v_{s,30}$ are over
60 and under conservative for deep sediments at short and long periods, respectively. Many
61 alternatives to $v_{s,30}$ are proposed to improve site soil characterization accounting for
62 additional information on the shear wave velocity profile with depth, the site dominant
63 frequency f_0 , the impedance contrast between sediments and bedrock and the depth to the
64 bedrock.

65 Various studies [11,12,17–21] propose new site classification based on a combination of these
66 different proxies. Gallipoli and Mucciarelli [21] and Cadet et al. [11] propose a two-
67 parameters site classification approach through the dominant frequency f_0 and the average

68 shear wave velocity $v_s(\bar{z})$ in the shallow soil up to the reference depth \bar{z} . Kotha et al. [17]
69 introduce a new approach classification characterized by the kernel density distributions of
70 $v_{s,30}$, $v_{s,10}$, H_{800} and the predominant period.

71 Recently, several researchers explore the performance of different site proxies in order to
72 reduce the aleatory variability on the seismic prediction. Derras et al. [14] investigate the
73 performance of four site condition proxies, $v_{s,30}$, f_0 , the topographical slope and the depth
74 H_{800} (the depth where the shear wave velocity v_s reaches 800 m/s) using a neural networks
75 approach, in order to assess their benefits to reduce the uncertainty of the site response. They
76 conclude that the best single-proxy is $v_{s,30}$ for periods below 0.6 s and f_0 or H_{800} at longer
77 periods and that the best pair is $(v_{s,30}, H_{800})$ at short periods and (f_0, H_{800}) at long periods.

78 Stambouli et al. [22] conduct a numerical investigation on 858 soil columns corresponding to
79 real sites profiles from Japan, USA, and Europe. They show that the best performing site
80 proxy is the impedance contrast between bedrock velocity and minimum surface velocity but
81 even the pair $(v_{s,30}, f_0)$ can reduce significantly the variability of the site response at least
82 around 60%.

83 Lately, Chuanbin et al. [23] study the best performing site proxies for the linear
84 characterization of the site response using 1840 ground-motion recordings from a KiK-net
85 database. They focus their study on the dominant period of the site T_0 , the site depths $Z_{0.8}$
86 and $Z_{1.0}$, which are measured site depths to layers having shear-wave velocity 0.8 and 1.0
87 km/s, respectively. They demonstrate that predictions based on the configuration using T_0 as
88 the primary and $v_{s,30}$ as the secondary proxy can induce a significant reduction in site-to-site
89 amplification variability.

90 Ciancimino et al. [24] adopt some classical proxies for site characterization in the context of

91 seismic site effect estimation. Their reliability is evaluated, under the assumption of linear
92 regime, and compared to the ground type classification adopted in the Eurocode 8 [25], New
93 Zealand Standard [26] and that suggested by Pitilakis et al. [18].

94 Following these recent reviews, the prediction of the seismic site response using only a single
95 proxy over the whole period range does not seem satisfactory. Hence, to improve the site
96 amplification estimation, it is advisable to use a combination of site proxies rather than a
97 single site proxy. Based on this idea, the goal of the present research is to assess the
98 correlation with the site amplification of some site parameters used to characterize the site
99 condition, with the aim of improving the expected ground motion prediction.

100 In this research, the site dominant frequency f_0 and the shear wave velocity gradient B_{30} are
101 selected as complementary proxies, in addition to $v_{s,30}$, and applied to a wide variety of soil
102 profiles with given $v_{s,30}$ and H_{800} . The two proposed proxies has been selected because they
103 can be estimated, without excessive cost, by geophysical methods applied to ambient
104 vibrations or seismic motions, recorded using temporary instruments located at the soil
105 surface [27].

106 Then, since the nonlinear behavior of soils has been recognized as an important factor in site
107 response [28,29], the second aim of this work is to explore how these site parameter proxies
108 allow to capture and account for the nonlinear component of site response.

109

110 **2. Methodology**

111 The stratigraphy of a set of soil profiles with a given average shear wave velocity in the upper
112 30m $v_{s,30}$ is randomly generated, according to the Monte Carlo method. Consequently, all the
113 generated profiles belong to the same ground type in the Eurocode classification [25].

114 The seismic wavefield along these soil profiles has been computed using the finite element
115 method (FEM) for spatial discretization and the Newmark algorithm for time discretization,

116 implemented in the SWAP_3C FEM package [30,31]. The highest-amplitude horizontal
117 component of a wide variety of recorded earthquakes, representative of regions of low to
118 moderate intensity, is applied as input motion at the base of each soil profile. These recorded
119 signals are propagated along each soil profile and the ground response at the surface is
120 evaluated in both cases of linear and nonlinear soil behavior.

121 Results are presented with regard to the amplification factors adopted by Ciancimino et al.
122 [24], in different period ranges, in order to distinguish short-, mid- and long-period
123 amplification factors. Differences between the response spectra of numerical signals at the
124 soil surface and the reference spectrum proposed by European buildings codes [25] are then
125 quantified and discussed.

126

127 **2.1 Set of generated soil profiles for the statistical analysis**

128 The parameters chosen for the set of soil profiles are the average shear wave velocity
129 $v_{s,30} = 270 \text{ m/s}$, corresponding to the ground type C according to the Eurocode 8 [25], the soil
130 depth of 30m, the number of layers equal to 4 and the density $\rho = 1850 \text{ kg/m}^3$. The
131 geotechnical properties assumed for the bedrock are the density $\rho_b = 2200 \text{ kg/m}^3$ and the
132 shear wave velocity $v_{sb} = 1000 \text{ m/s}$.

133 The properties of each layer are generated considering each stochastic parameter uniformly
134 distributed in a given range. The soil layer thickness ranges in $[1-15 \text{ m}]$, the shear wave
135 velocity in $[100-800 \text{ m/s}]$ and 4 soil types can be randomly targeted.

136 Each soil type from 1 to 4 is associated to a plasticity index $PI = 0, 5, 10$ and 20% ,
137 respectively. Yokota et al. [32] have shown that normalized shear modulus reduction curve
138 for different types of soils can be expressed by a set of formulas in the absence of available
139 test data. To this regard, a normalized shear modulus reduction curve, as a function of the

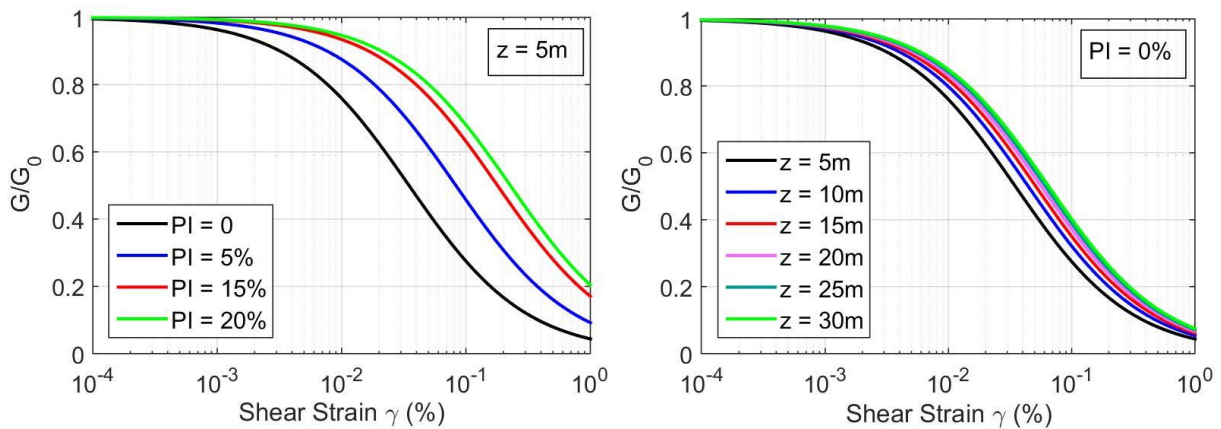
140 shear strain γ , is derived using the four-parameter model proposed by Darendeli [33] to
 141 characterize normalized modulus reduction formulation:

$$142 \quad G(\gamma)/G_0 = 1 / \left[1 + (\gamma/\gamma_r)^\alpha \right] \quad (1)$$

143 assuming a normal consolidated soil (over-consolidation ratio $OCR=1$). The reference shear
 144 strain is defined as $\gamma_r = (\phi_1 + \phi_2 \cdot PI \cdot OCR^{\phi_3}) \sigma_{v0}'^{\phi_4}$, where from ϕ_1 to ϕ_4 are parameters that
 145 relate the normalized modulus reduction curve to soil type and loading conditions estimated
 146 on the basis of statistical analysis ($\phi_1 = 0.0352$, $\phi_2 = 0.001$, $\phi_3 = 0.3246$, $\phi_4 = 0.3483$) and
 147 $\alpha = 0.92$.

148 The vertical effective stress σ_{v0}' is calculated each 5m using the chosen soil density
 149 $\rho = 1850 \text{ kg/m}^3$, to account for the variation of the shear modulus decay curve with depth.

150 The normalized shear modulus reduction curves employed for the four soil types, associated
 151 to a different plasticity index PI are shown in Fig. 1 (a), for a fixed depth $z = 5 \text{ m}$. The curves
 152 $G(\gamma)/G_0$ at various depths, associated to a related vertical effective stress σ_{v0}' , for the soil
 153 type 1 having plasticity index $PI = 0$, are shown in Fig. 1 (b).



154
 155

(a)

(b)

156 Fig. 1. Normalized shear modulus reduction curves obtained by Darendeli formulation [33]
 157 (a) for the four soil types associated to different plasticity index PI and a given depth $z = 5 \text{ m}$,

158 (b) and for increasing depth z and a given plasticity index $PI = 0$.

159

160 A set of 300 soil profiles is randomly generated with different layer thicknesses and
161 impedance contrasts, in order to represent various site conditions and estimate the influence of
162 their uncertainty on the amplification process. Among these 300 soil profiles, for 200 of
163 them, the shear wave velocity profile increases with depth to consider the effect of increasing
164 confining stresses. In the other 100 soil profiles, there is an inversion of the shear wave
165 velocity profile in one of the middle layers. The position and the thickness of the layer with
166 the shear wave velocity inversion are selected randomly.

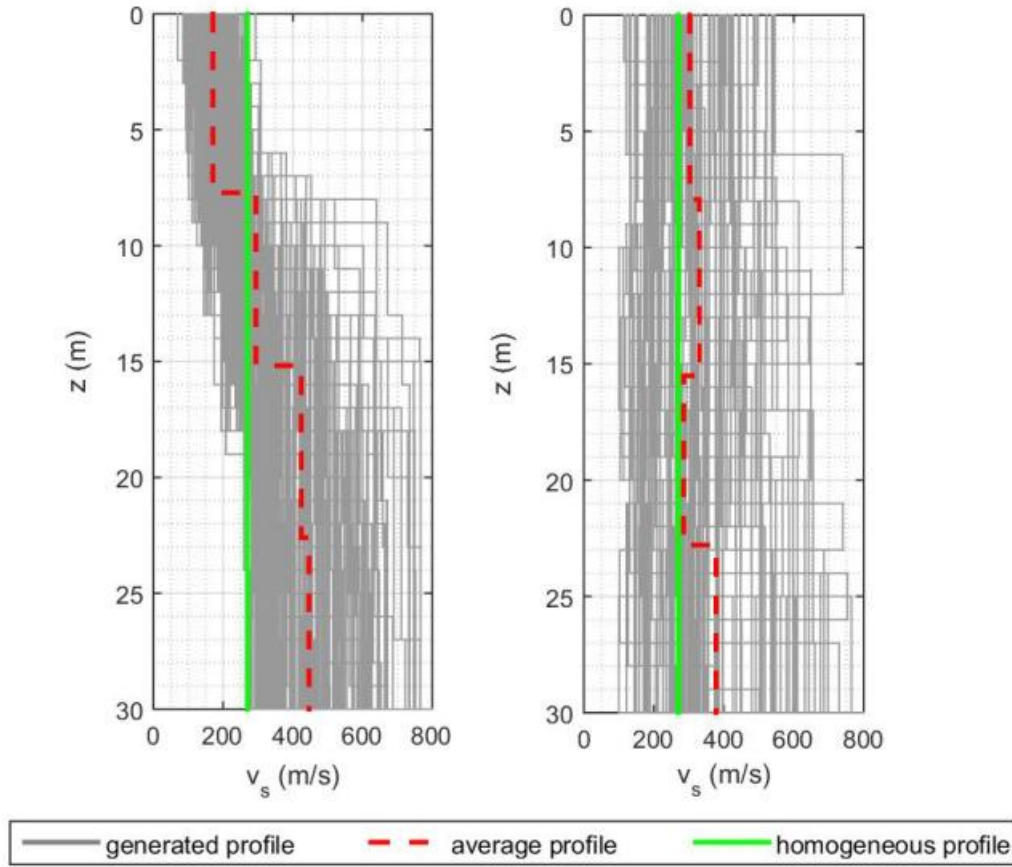
167 The generated shear wave velocity profiles with depth $v_s(z)$ are shown in Fig. 2, in the cases
168 of increasing v_s and of inversions in the profile (a and b, respectively). It can be noted that the
169 variability in the shear wave velocity profile, according to the same $v_{s,30} = 270 \text{ m/s}$, can be
170 very large.

171

172 **2.2 Set of recorded seismic motions**

173 A set of 40 signals, recorded at rock outcrops, is selected as input for the computation of the
174 seismic wave propagation along the 300 generated soil profiles. These seismic motions
175 originate from ITACA, the Italian Strong Motion Database [34], ISESD, European Strong
176 Motion Database [35] or PEER, Pacific Earthquake Engineering Research Center Database
177 [36].

178 In the adopted set of seismic signals, 20 of them are representative of low to moderate
179 intensity with magnitudes ranging from 3 to 5.5 (associated to the type 2 response spectrum of
180 Eurocode 8 [25]) and the other 20 are representative of moderate to high seismicity with
181 magnitude ranging from 5.6 to 7.5 (type 1 response spectrum).



182

183

184 Fig. 2. Generated shear wave velocity profiles with depth $v_s(z)$ in the cases of (a) increasing
 185 v_s and (b) shear wave velocity inversion. All the generated soil profiles have the same
 186 average shear wave velocity $v_{s,30} = 270$ m/s .

187

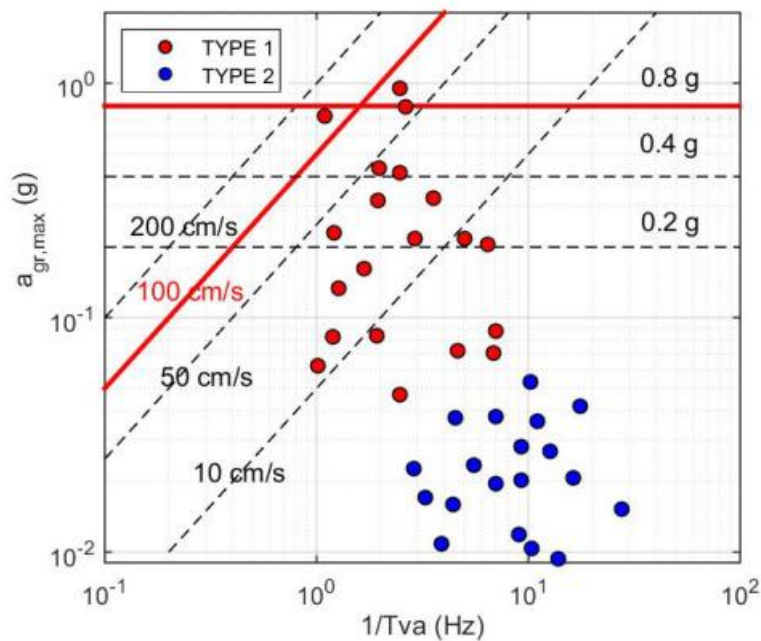
188 Taking into account the influence of the frequency content on the free-field (FF) ground
 189 motion, the selected seismic records are representative of a wide variety of dominant
 190 frequencies. The set of recorded seismic motions is sorted in terms of frequency content using
 191 the equivalent period T_{VA} , parameter proposed by Cameron and Green [37], defined as

$$192 \quad T_{VA} = 2\pi \frac{\alpha_V(\xi = 5\%) v_{gR}}{\alpha_A(\xi = 5\%) a_{gR}} \quad (2)$$

193 where a_{gR} and v_{gR} are the peak ground acceleration and velocity at the outcrop, respectively.

194 The median spectrum amplification factors for horizontal motion are estimated by Newmark
 195 and Hall [38] as $\alpha_A(\xi=5\%)=2.12$ and $\alpha_V(\xi=5\%)=1.65$, for the constant acceleration and
 196 constant velocity regions of 5% damped response spectra, respectively.

197 Fig. 3 shows the equivalent predominant frequency $1/T_{VA}$ related with the peak ground
 198 acceleration on rock outcrop a_{gR} for the set of 40 seismic motions. The oblique lines represent
 199 uniform values of v_{gR} . The severity of seismic motion increases according to the direction of
 200 increasing velocity (from the bottom-right corner toward the top-left one, where the values of
 201 a_{gR} and v_{gR} are both higher). Based on the observations in Kobe [39], the values $a_{gR} = 0.8g$
 202 and $v_{gR} = 100\text{cm/s}$ are considered as risk limits, meaning that the input motions above these
 203 values are considered as the most severe ones (Fig. 3). Then the set of the selected seismic
 204 motions is made up of a wide variety of frequency content, peak acceleration and peak
 205 velocity.



206
 207 Fig. 3. Equivalent predominant frequency T_{VA} related to the peak ground acceleration at the
 208 outcrop a_{gR} for the set of 40 seismic motions. The oblique lines represent uniform values of

209 v_{gR} . The horizontal lines represent constant values of a_{gR} .

210

211 **2.3 Wave propagation model**

212 Assuming a vertical propagation in a horizontally layered medium, the numerical analysis is
213 undertaken as a one-dimensional approach. The soil is assumed homogeneous and both
214 assumptions of linear and nonlinear constitutive behavior are analyzed.

215 Quadratic line finite elements are adopted for spatial discretization and the Newmark
216 algorithm for time discretization, with some numerical damping. The SWAP_3C finite
217 element software [30,31,40,41] is used for the numerical simulations.

218 At the soil-bedrock interface, an absorbing boundary condition adopted by Joyner and Chen
219 [42] is applied in order to take into account the elasticity of the underlying bedrock and allow
220 energy to be radiated back. The mechanical properties characterizing the bedrock are the
221 density ρ_b and the shear wave velocity v_{sb} .

222 The largest horizontal component of the signal recorded at the reference outcrop is halved and
223 imposed as the incident wave at the soil-bedrock interface.

224 The finite element size in each soil layer is defined as the minimum between 1m and one
225 tenth of the minimum wavelength, related to shear wave velocity in the layer and the
226 maximum frequency assumed equal to 15Hz, above which the spectral content of the input
227 signal is considered negligible.

228 Details of the finite element model employed in this research are completely described by
229 Santisi d'Avila et al. [30,31].

230

231 **2.4 Hysteretic model for soil**

232 The so-called Masing-Prandtl-Ishlinskii-Iwan (MPII) nonlinear constitutive model [43] is
233 used for the soil in a total stress analysis. Its main feature is the satisfactory reproduction of

234 nonlinear and hysteretic behavior of soils under cyclic loadings [40,41], starting from the
235 knowledge of a small number of parameters characterizing the soil properties, such as elastic
236 parameters and the shear modulus reduction curve.

237 The MPII model is elasto-plastic with linear kinematic hardening. The plasticity model
238 assumes an associated plastic flow, which allows for isotropic yield. This rheological model
239 has no viscous damping and the soil damping is purely hysteretic and not frequency
240 dependent. The size of the Von Mises yield surface is imposed by the backbone curve in the
241 uniaxial stress case. The tangent constitutive matrix is deduced from the actual strain level
242 and the strain and stress values at the previous time step [43,44]. [44] This means that the
243 stress level depends on the strain increment and strain history but not on the strain rate.

244

245 **2.5 Data analysis**

246 An optimal selection of site parameters is an important tool for the prediction of the expected
247 ground motion. Based on recent results [14,22–24], the site dominant frequency f_0 and the
248 shear wave velocity gradient B_{30} are chosen as complementary proxies in this study.

249 As proposed by Regnier et al. [45], the shear wave velocity gradient B_{30} is defined as the
250 slope of the linear regression of the relation between the logarithm of the shear wave velocity
251 profile $v_s(z)$ and the depth z . Thus, it is computed as:

$$252 \quad \log(v_s(z)) = B_{30} \log(z) + A_{30} \pm \sigma_{30} \quad (3)$$

253 where A_{30} is the vertical intercept of the regression, σ_{30} is the standard deviation associated to
254 the linear regression.

255 The shear wave velocity gradient B_{30} , estimated by Eq. (3) for all the generated 30m deep
256 soil profiles, quantifies the variation of the shear wave velocity $v_s(z)$ contrast in the
257 superficial layers. Its value is close to zero if the velocity is nearly constant with depth and it

258 is larger if the shear wave velocity v_s increases rapidly with depth [45].

259 The results of the numerical simulations of seismic wave propagation in the set of generated
260 soil profiles, are first analyzed in terms of amplification factors, according to Ciancimino et
261 al. [24], in both cases of linear and nonlinear soil behavior.

262 The soil amplification factor S_s is a local indicator of the site amplification, providing an
263 estimate of the site effect on the FF motion. It is defined as the ratio of the peak ground
264 acceleration at the surface a_g to the peak acceleration at the outcrop a_{gR} :

$$265 \quad S_s = a_g / a_{gR} \quad (4)$$

266 The spectral amplification factor SA and the spectral velocity factor SV are used to quantify
267 the ground motion intensity in a given period range. These parameters are proposed by Rey et
268 al. [46]. They are defined as the ratio of I_{soil} to I_{rock} . These are the intensity of the spectrum
269 estimated using the signal at the ground surface and at the outcrop, respectively. The
270 intensities used in the amplification factors SA and SV are calculated by Housner [47] using
271 the spectrum in terms of acceleration $PSA(T)$ and velocity $PSV(T)$, respectively, as
272 follows:

$$273 \quad SA = \frac{I_{soil}}{I_{rock}} \quad \text{with} \quad I = \int_{T_1}^{T_2} PSA(T) dT \quad (5)$$

$$274 \quad SV = \frac{I_{soil}}{I_{rock}} \quad \text{with} \quad I = \int_{T_1}^{T_2} PSV(T) dT \quad (6)$$

275 In Eqs (5) and (6), $[T_1 - T_2]$ is the fixed range of vibration period.

276 In this research, the spectra $PSA(T)$ and $PSV(T)$ are normalized with respect to the peak
277 acceleration at the outcrop a_{gR} . The period range $[0.05 - 2.5s]$, representative of the
278 fundamental vibration period for more common structures, is divided into three sub-ranges in
279 order to analyze the results for short, middle and long periods of vibration. Spectral

280 amplification factors for short [0.05–0.5s], middle [0.5–1s] and long [1–2.5s] periods of
281 vibration are indicated as (SA_S, SV_S) , (SA_M, SV_M) and (SA_L, SV_L) , respectively.

282 In a second phase, the response spectra of numerical FF motion are compared to those
283 suggested by Eurocode 8 [25]. Finally, the results in terms of site amplification factors are
284 compared with the Eurocode 8 [25], the New Zealand Standard [26] building codes, and those
285 evaluated by Pitilakis et al. [18], Ciancimino et al. [24].

286

287 **3. Results and discussion**

288 The variability of the shear wave velocity profiles with depth $v_s(z)$ for the set of generated
289 soil profiles, having the same average $v_{s,30} = 270$ m/s, is shown in Fig. 2. The FF motion
290 obtained by numerical simulation, propagating the set of recorded seismic signals along the
291 generated soil profiles is analyzed.

292 In the following, the influence on site amplification of complementary parameters as the shear
293 wave velocity profiles with depth $v_s(z)$, the site dominant frequency f_0 and the shear wave
294 velocity gradient B_{30} is assessed. The fluctuation of amplification factors with the site
295 parameters f_0 and B_{30} is analyzed.

296

297 **3.1 Site parameter variability**

298 The dominant frequency of the site f_0 is obtained by evaluating the FF to bedrock transfer
299 function (TF) that is the ratio of the Fourier spectrum of the accelerograms at the FF soil
300 surface and at the outcropping bedrock surface. A low-amplitude signal is used so that the soil
301 remains in the elastic regime. The frequency corresponding to the peak of this TF corresponds
302 to the fundamental frequency of the soil column, considered as the dominant frequency of the
303 site f_0 . In the case of a homogeneous soil, the fundamental frequency of a 30m deep soil

304 profile, having a shear wave velocity $v_s = 270 \text{ m/s}$, is also deduced [48] as
305 $f_0 = v_s / (4H) = 2.25 \text{ Hz}$. The homogeneous soil profile is adopted in the following
306 comparisons as canonical case.

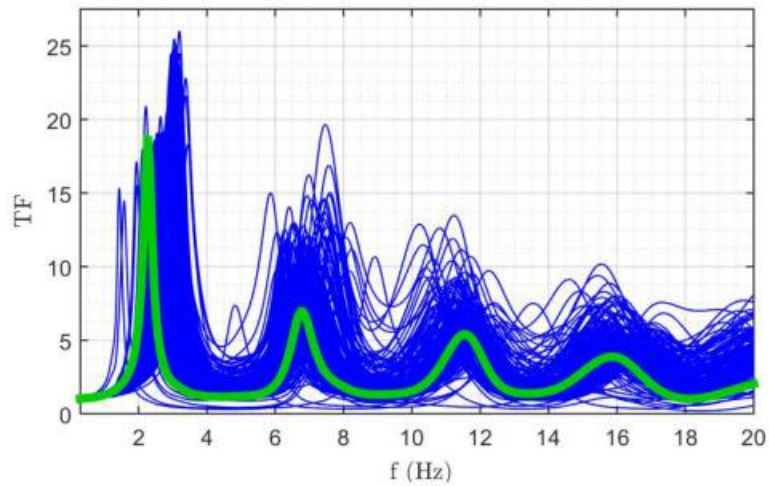
307 Fig. 4 displays the TF obtained for the soil profile with a homogeneous soil, the generated soil
308 profiles with increasing shear wave velocity with depth $v_s(z)$ and those with an inversion in
309 the $v_s(z)$ profile. The dominant frequency of the site f_0 , obtained for the set of all the
310 generated soil profiles ranges from 1.5 to 3.5 Hz. For increasing $v_s(z)$ profiles (Fig. 4a), the
311 dominant frequency of the site is mostly higher than the frequency for the homogeneous case.
312 Whereas the natural frequencies obtained for soil profiles with an inversion in $v_s(z)$ are
313 distributed in a frequency range (Fig. 4b). The peaks of the TF obtained for the generated soil
314 profiles show a higher amplification compared with the homogeneous soil profile in most
315 cases. In particular, the amplification estimated for the soil profiles having increasing $v_s(z)$ is
316 larger for higher f_0 (Fig. 4a).

317 According to Fig. 4, the site amplification changes depending on the stratigraphy (i.e. shear
318 wave profile with depth $v_s(z)$) and the fundamental frequency of the site f_0 . The frequency
319 content of the surface motion varies accordingly.

320 Fig. 5 illustrates the linear correlation between the shear wave velocity gradient B_{30} and the
321 fundamental frequency of the site f_0 , for the set of generated soil profiles with given $v_{s,30}$.
322 This correlation is high, with a correlation coefficient $r^2 = 0.85$, for the whole set of 300 soil
323 profiles.

324 The amplification factors in Eqs (4), (5) and (6) are calculated using the computed FF motion
325 and the related response spectrum for all the 24000 samples (set of 40 recorded seismic
326 signals applied to 300 generated soil profiles, for linear and nonlinear soil behaviors).

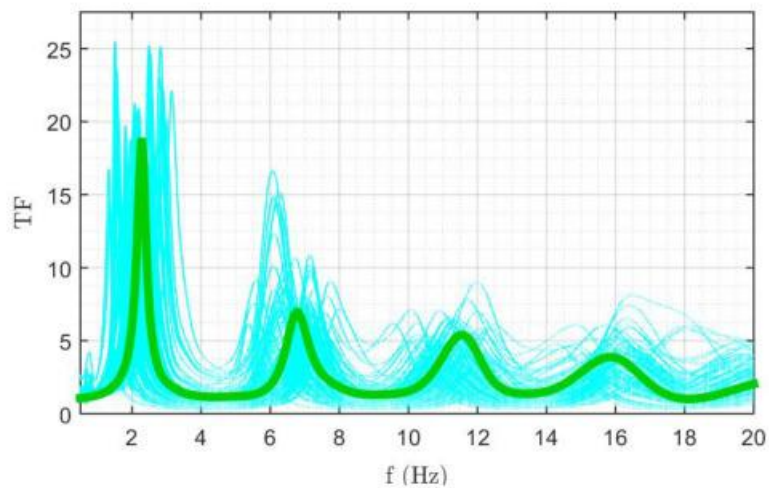
327 The estimated amplification factors S_s , SA and SV , SA_s , SA_M and SA_L , SV_s , SV_M and SV_L ,
328 are shown in Figs 6, 7, 8, and 9 as functions of the dominant period of the site $T_0 = 1/f_0$ and
329 of the shear wave velocity gradient B_{30} , respectively, for both cases of linear (a) and nonlinear
330 (b) behavior. The trend of mean and standard deviation is also displayed by the thick and
331 dashed lines, respectively.



332

333

(a)



334

335

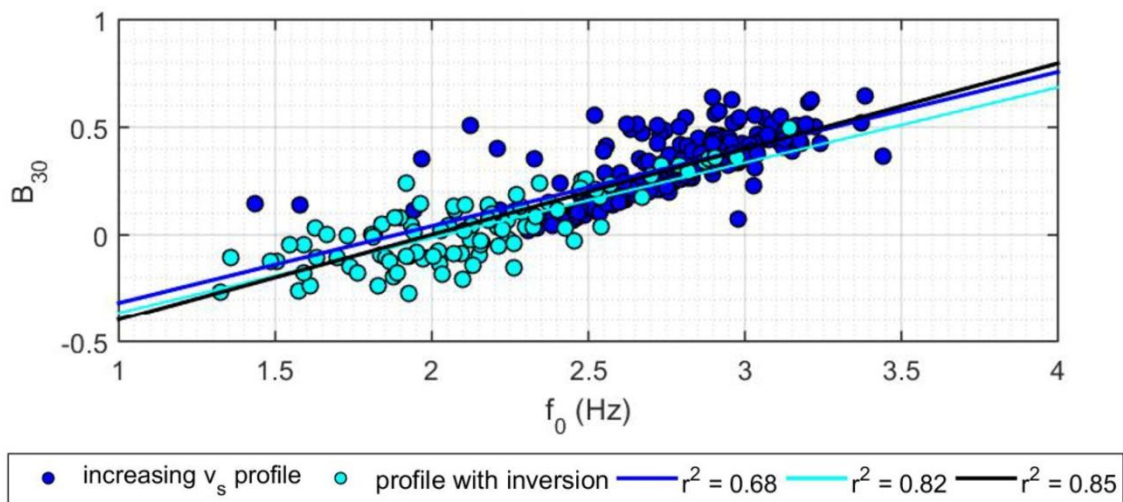
(b)

336 Fig. 4. Free-field to bedrock transfer function for the generated deep soil profiles having
337 increasing shear wave velocity profile (a) and showing a velocity inversion (b). The thick line
338 is the transfer function for the homogeneous soil profile.

339

340 Figs 6, 7, 8 and 9 illustrate the amplification factors in the three fixed ranges of period in
341 order to understand if their variation is modified for different periods. It appears that the
342 largest amplifications are reached for short vibration periods (lower than 0.5 s).

343 Figs 6 and 8 display that site amplification is strongly dependent on the site predominant
344 period T_0 , for short vibration periods of the FF motion (SA_S, SV_S) and independent from it for
345 long periods (SA_L, SV_L). Moreover, site amplification is much more pronounced in soil
346 profiles having T_0 lower than that of the homogeneous profile, for short vibration periods of
347 the FF motion (SA_S, SV_S). Whereas, for middle periods of vibrations (SA_M, SV_M), site
348 amplification is more pronounced in soil profiles having predominant period T_0 higher than
349 that of the homogeneous profile.

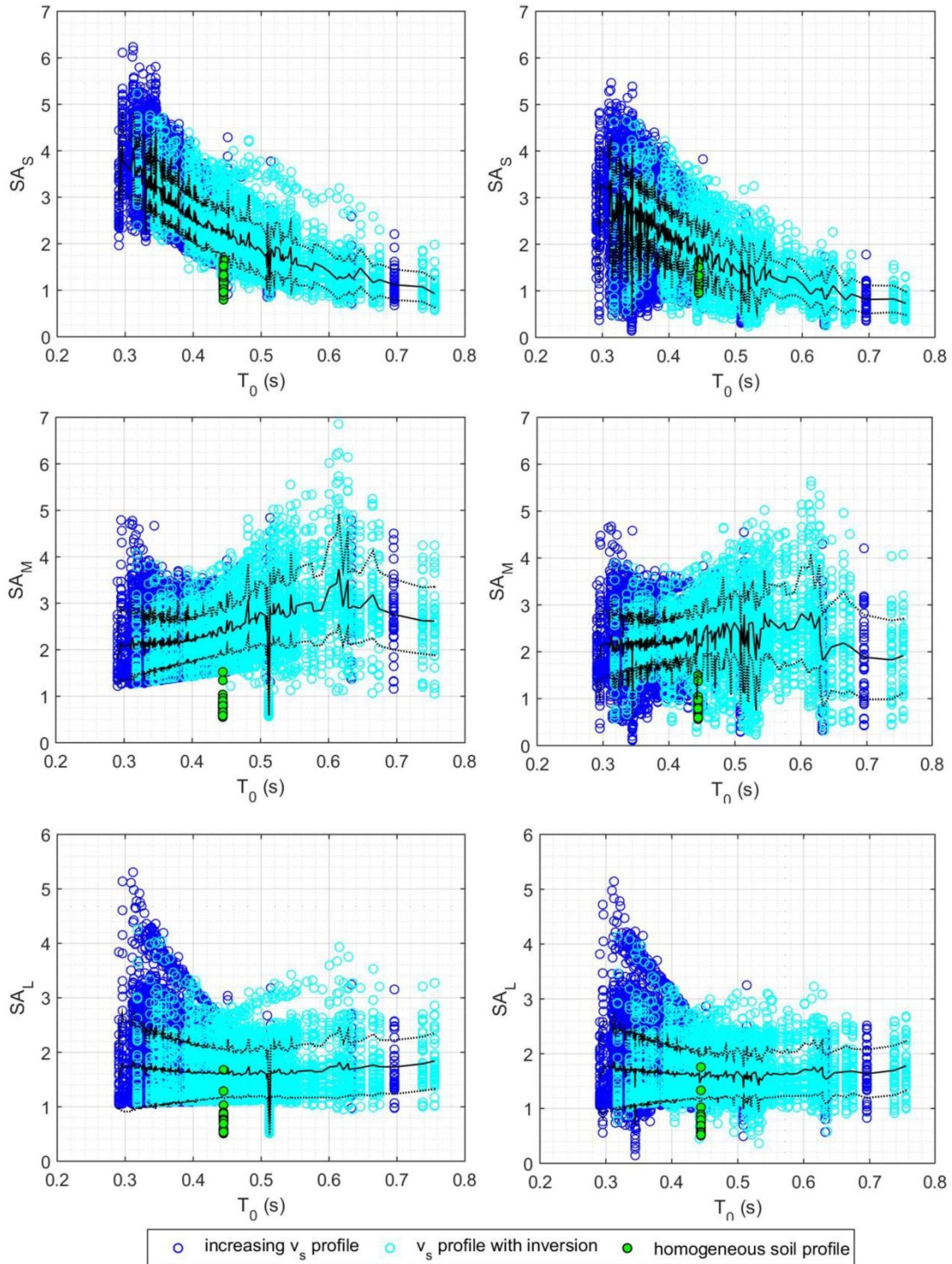


351 Fig. 5. Linear regression of the shear wave velocity gradient B_{30} with reference to the
352 fundamental frequency of the site f_0 , for the generated deep soil profiles. The thick line is for
353 the set of all 300 generated soil profiles.

354

355 Figs 7 and 9 show that the largest values of amplification factors are reached for short

356 vibration periods of the FF motion (SA_S, SV_S), lower than 0.5 s, in soil profiles having a high
 357 shear wave velocity gradient B_{30} , which corresponds to sites with a large impedance contrast
 358 in the first 30 m or with a steep slope in shear wave velocity profile.



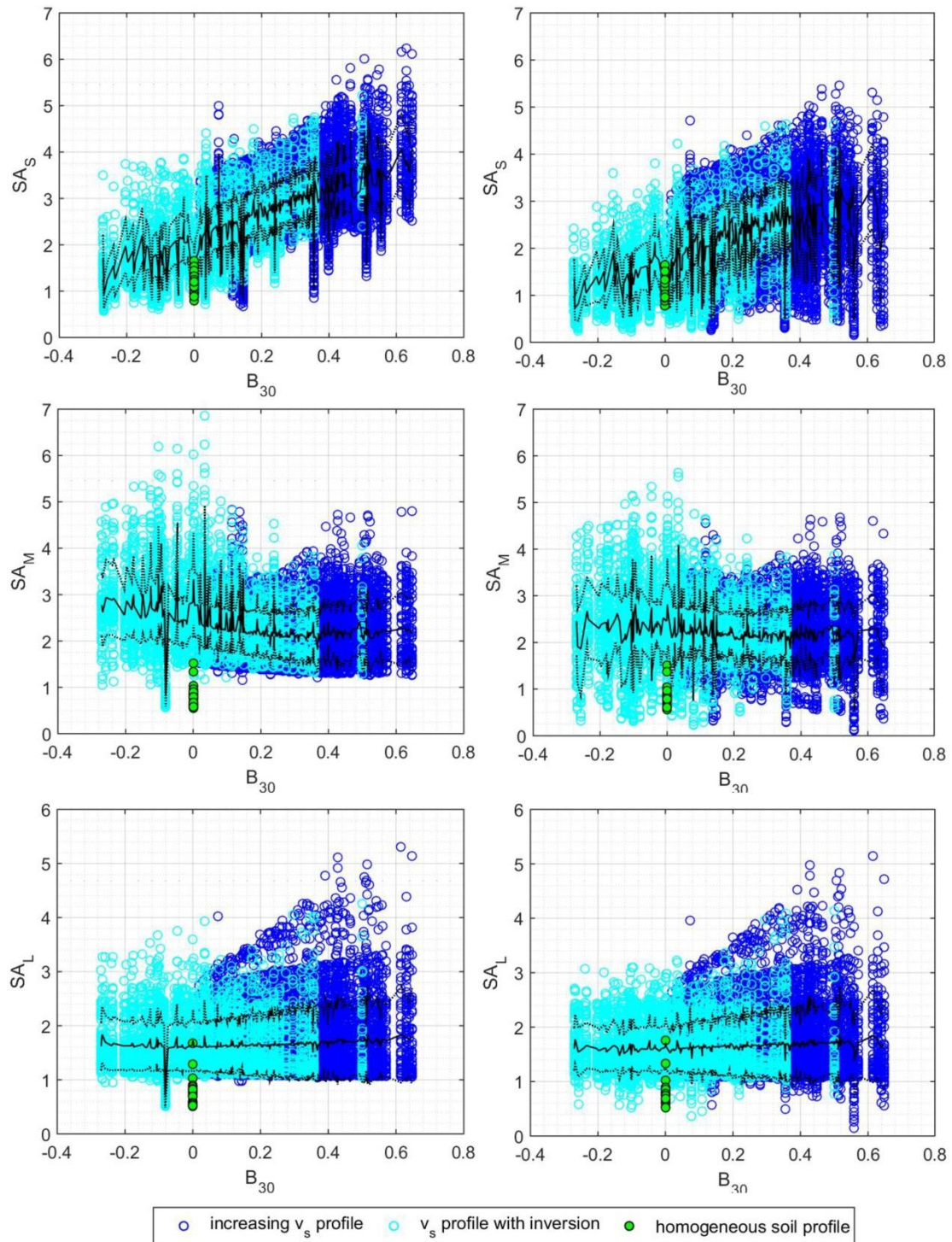
359

360

(a)

(b)

361 Fig. 6. Amplification factors SA_S , SA_M and SA_L as a function of the dominant period of the
 362 site T_0 , for both cases of linear (a) and nonlinear (b) behaviors. The thick and dashed lines
 363 represent the mean and means plus one standard deviation (SD) trend.



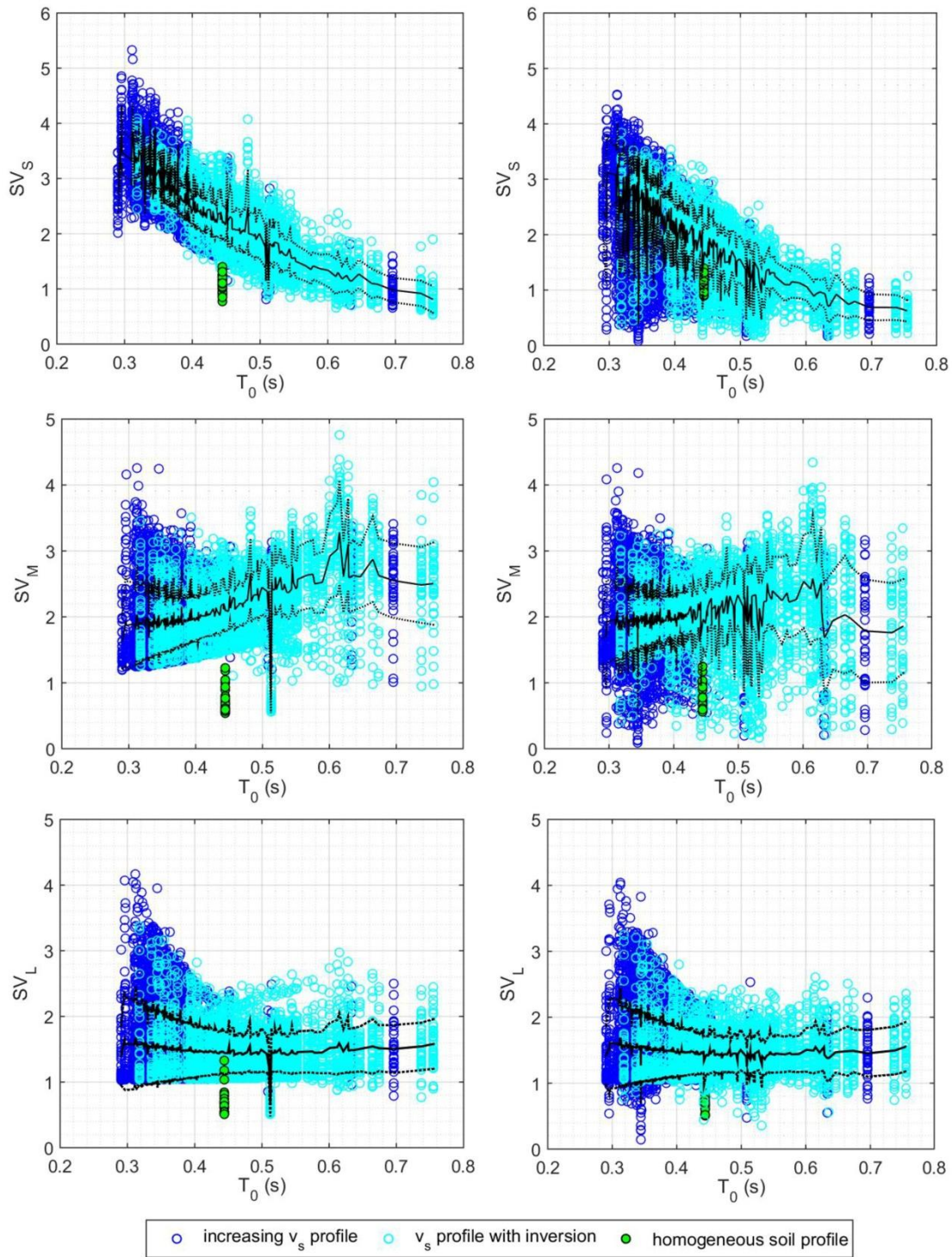
364

365

(a)

(b)

366 Fig. 7. Amplification factors SA_S , SA_M and SA_L as a function of the shear wave velocity
 367 gradient B_{30} , for both cases of linear (a) and nonlinear (b) behaviors. The thick and dashed
 368 lines represent the mean and means plus one standard deviation (SD) trend.



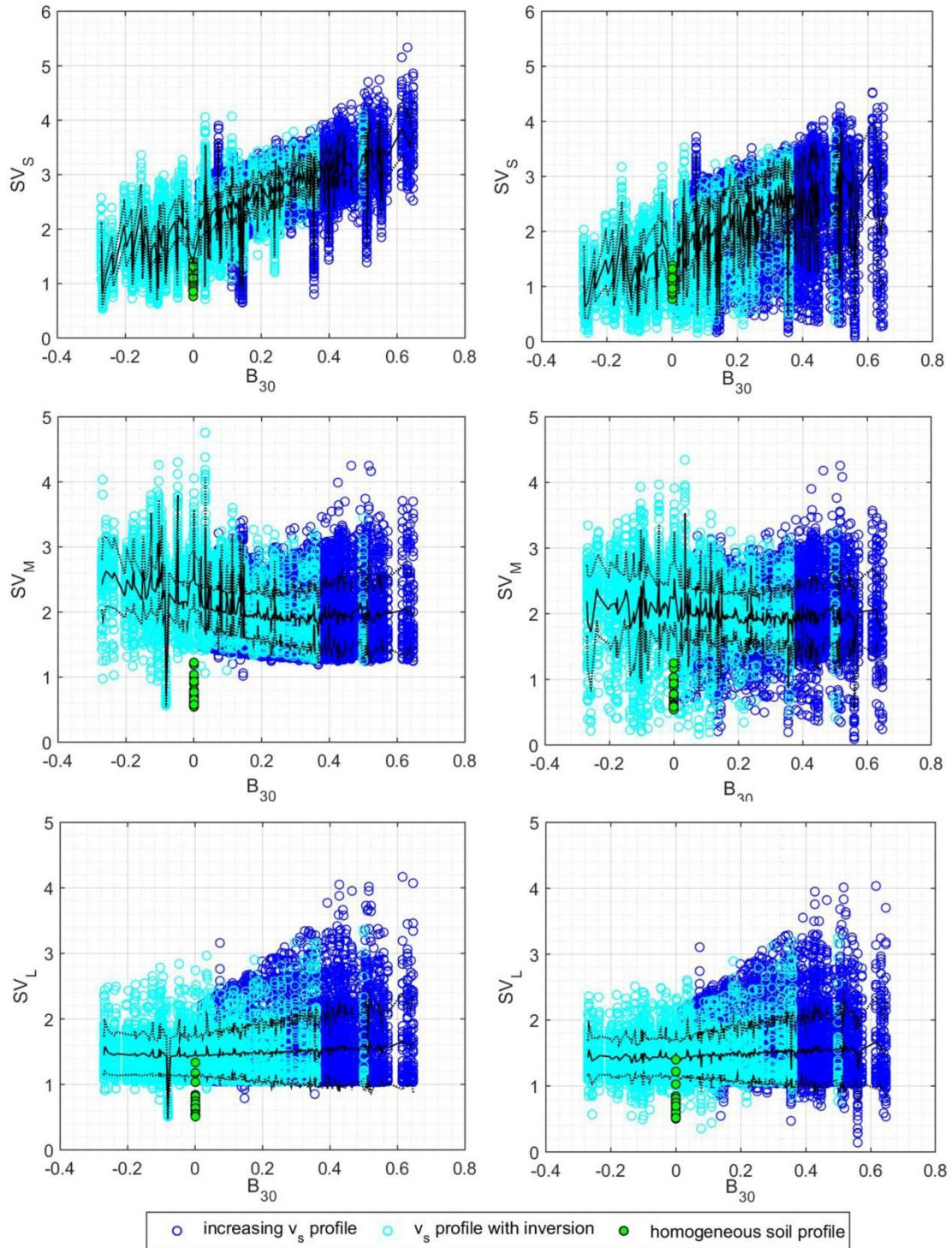
369

370

(a)

(b)

371 Fig. 8. Amplification factors SV_S, SV_M and SV_L as a function of the dominant period of the
 372 site T_0 , for both cases of linear (a) and nonlinear (b) behaviors. The thick and dashed lines
 373 represent the mean and means plus one standard deviation (SD) trend.



374

375

(a)

(b)

376 Fig. 9. Amplification factors SV_S , SV_M and SV_L as a function of the shear wave velocity
377 gradient B_{30} , for both cases of linear (a) and nonlinear (b) behaviors. The thick and dashed
378 lines represent the mean and means plus one standard deviation (SD) trend.
379 The nonlinear soil behavior on the site response induces a reduced amplification effect.
380 Similarly to the case of linear soil behavior, the site amplification is more pronounced in the
381 case of short vibration periods of the FF motion and it is strongly dependent on the proposed
382 site parameters. On the contrary, the site amplification is less pronounced and independent
383 from the proposed site parameters, for longer vibration periods of the FF motion.

384

385 **3.2 Influence on site effects of the nonlinear soil behavior**

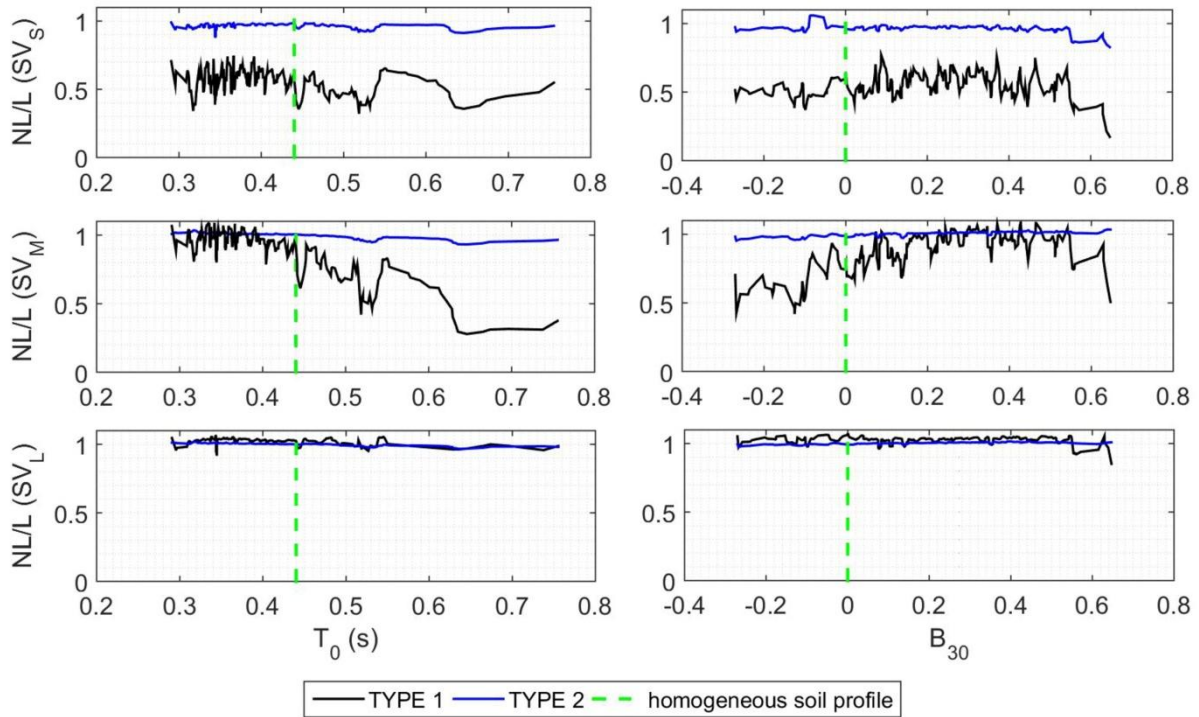
386 In this section, the effects of soil nonlinearities on site response are investigated with
387 reference to the proposed site proxies (predominant period T_0 and shear wave velocity
388 gradient B_{30}). The main goal is to verify the reliability of T_0 and B_{30} even in the range of soil
389 nonlinear behavior. The impact of nonlinear soil response on the site response is characterized
390 in terms of amplification factor SV . The SV factor is estimated in both cases of linear and
391 nonlinear soil response, in the three adopted period ranges. The amplification factor NL/L is
392 computed as the ratio of spectral velocity factors SV_S , SV_M and SV_L in the ranges of short,
393 middle and long period, for nonlinear soil behavior to that for linear soil behavior.

394 Fig.10 illustrates the average amplification factor as a function of the site dominant period T_0
395 (Fig. 10a) and shear wave velocity gradient B_{30} (Fig. 10b). Results are distinguished between
396 those for weak earthquakes (associated to the type 2 response spectrum of Eurocode 8 [25])
397 and strong earthquakes (type 1 response spectrum).

398 As expected, the effect of nonlinear soil behavior is negligible for small earthquakes (type 2
399 response spectrum of Eurocode 8 [25]) for the whole range of periods of vibration. In fact, the

400 NL/L ratio is close to one.

401 In the case of stronger earthquakes (type 1 response spectrum), the modification in the site
402 response depends on the stratigraphy and varies with the vibration period of the FF motion.



403

404

405 Fig. 10. Computed ratio of spectral velocity factors SV_S , SV_M and SV_L (short, intermediate
406 and long periods of vibration) for nonlinear soil behavior to that for linear soil behavior
407 (NL/L) as a function of the dominant period of the site T_0 (a) and the shear wave velocity
408 gradient B_{30} (b), for the whole set of generated soil profiles. The curves are distinguished
409 between those for small earthquakes (associated to the type 2 response spectrum of Eurocode
410 8) and strong earthquakes (type 1 response spectrum).

411

412 According to Fig. 10, for vibration periods of the strong motion over 1s, the effect of
413 nonlinear soil behavior is negligible (see SV_L). On the contrary, in the range of short periods
414 (see SV_S), the amplitude reduction due to nonlinear effects is up to 60%. Moreover, the

415 amplification factor in the range of middle periods (see SV_M) show a remarkable amplitude
416 reduction for a site predominant period T_0 higher than 0.44s (period of vibration of the
417 homogeneous soil profile) and a reduction up to 10% for lower periods T_0 (Fig 10a). An
418 important amplitude reduction is obtained for a shear wave velocity gradient B_{30} outside the
419 range $[0-0.5]$, that correspond to soil profiles with significant impedance contrast (high B_{30})
420 and velocity inversions (negative B_{30}).

421

422 **3.4 Comparison with building codes**

423 Fig. 11 displays the comparison of the average pseudo-acceleration response spectrum
424 normalized with respect to the peak acceleration of the outcropping motion, using a damping
425 ratio of 5% .

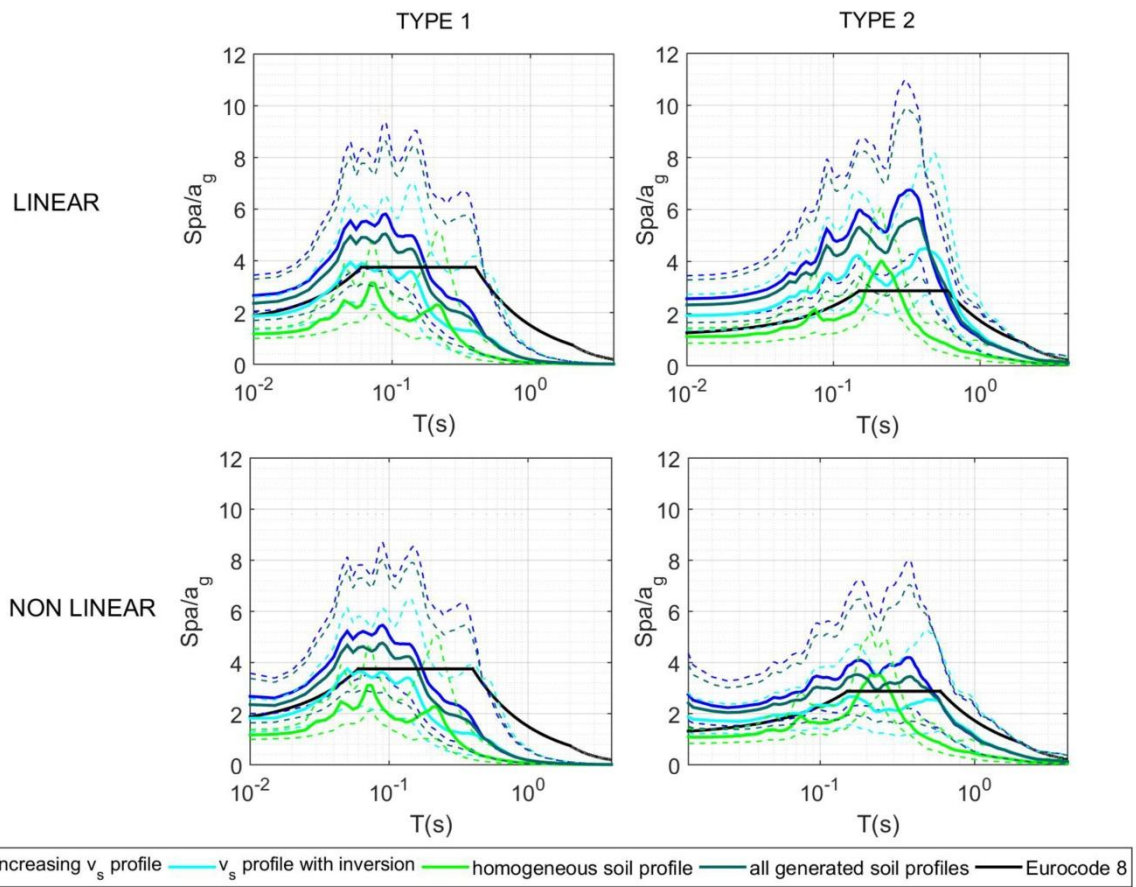
426 The linear and nonlinear computations are separated and, for both, the cases of weak
427 earthquakes (associated to the type 2 response spectrum of the Eurocode 8 [25]) and strong
428 earthquakes (type 1 response spectrum) are distinguished. In each of these combinations, the
429 average pseudo-acceleration response spectra are estimated for the FF motion in the case of
430 increasing shear wave velocity and for profiles with a velocity inversion.

431 The elastic response spectra proposed by Eurocode 8 is conservative, compared to the
432 obtained average response spectra, for higher periods (higher than 0.2s for type 2 and 0.6s
433 for type 1). Conversely, for lower periods, the average response spectrum, obtained for all the
434 generated soil profiles, gives higher acceleration peaks.

435 If the elastic response spectrum proposed by Eurocode 8 [3] is compared for the spectrum in
436 the homogeneous case, with average soil properties, it is conservative for the whole ranges of
437 period for weak earthquakes (type 2) and in most cases for strong earthquakes (type 1).

438 The reduction of the site response for the nonlinear soil behavior is negligible for weak

439 earthquakes (type 2) and significant for strong earthquakes (type 1).



440

441

442

443

444

445

446

447

448

449

450

451

452

(a) (b)

Fig. 11. Mean (solid line) acceleration response spectra (damping ratio of 5%) and mean plus one standard deviation (dashed line), evaluated for the free-field motion of the generated multilayered soil profiles, compared to the homogeneous case and the elastic response spectrum proposed by Eurocode 8 [3]. The cases are distinguished as follows: assumption of linear and nonlinear soil behavior; weak earthquakes (a) and strong earthquakes (b). Following the approach adopted by Ciancimino et al. [24] for the linear regime, the site amplification factors are evaluated for the samples of the present statistical analysis, in the case of linear and nonlinear soil behavior. The computed amplification factors are compared with those suggested by Eurocode 8 [25] and New Zealand Standard [26] building codes, with those proposed by Pitilakis et al. [18] and with those obtained by Ciancimino et al. [24]. The ground type classification used in the Eurocode 8 [25] is only based on the $v_{s,30}$ parameter. In

453 the New Zealand Standard [26], the fundamental site period is included as a proxy of site
454 effects. In addition, Pitilakis et al. [18] classify the ground type using the fundamental period
455 of the site, the depth of the seismic bedrock and the average soil column shear wave velocity
456 are taken into account. The 300 generated soil profiles are identified as ground type C
457 according to Eurocode 8 [25] and as C2 according Pitilakis et al. [18]. Among them, 286 are
458 identified as ground type C according to the New Zealand Standard [26] building codes
459 ($T_0 > 0.6s$).

460 The comparison between the mean value of site amplification factors S_s (Eq. (4)) and SA
461 (Eq. (5)), and the values within one standard deviation of the mean are represented in Fig. 12
462 for weak earthquakes and in Fig. 13 for strong earthquakes. These values are compared to
463 those obtained according to the building codes to analyze their reliability. The coefficient of
464 variation CV of S_s and SA is also calculated. In each figure, the simulations under the
465 assumption of linear and nonlinear soil behavior are separated. The amplification factors are
466 estimated, for both soil behaviors, using only the FF motions of multilayered soil profiles with
467 increasing shear wave velocity with depth, only the FF motions of soil profiles with a velocity
468 inversion, the FF motions of all the generated soil profiles and the FF motion of the
469 homogeneous soil profile.

470 The obtained numerical results obtained under the assumption of linear soil behavior are also
471 compared to those obtained by Ciancimino et al. [24], that performed analyses on a database
472 of seismic responses of one-dimensional soil profiles having equivalent linear behavior. We
473 can observe that our results under the assumption of linear behavior are in good agreement
474 with those obtained by Ciancimino et al. [24].

475 According to Figs 12 and 13, only the amplification factors obtained for the case of
476 homogeneous soil profile are smaller than those suggested by Eurocode 8 [25] and the same
477 consideration is made comparing with the New Zealand Standard [26] building codes (Fig.

478 14).

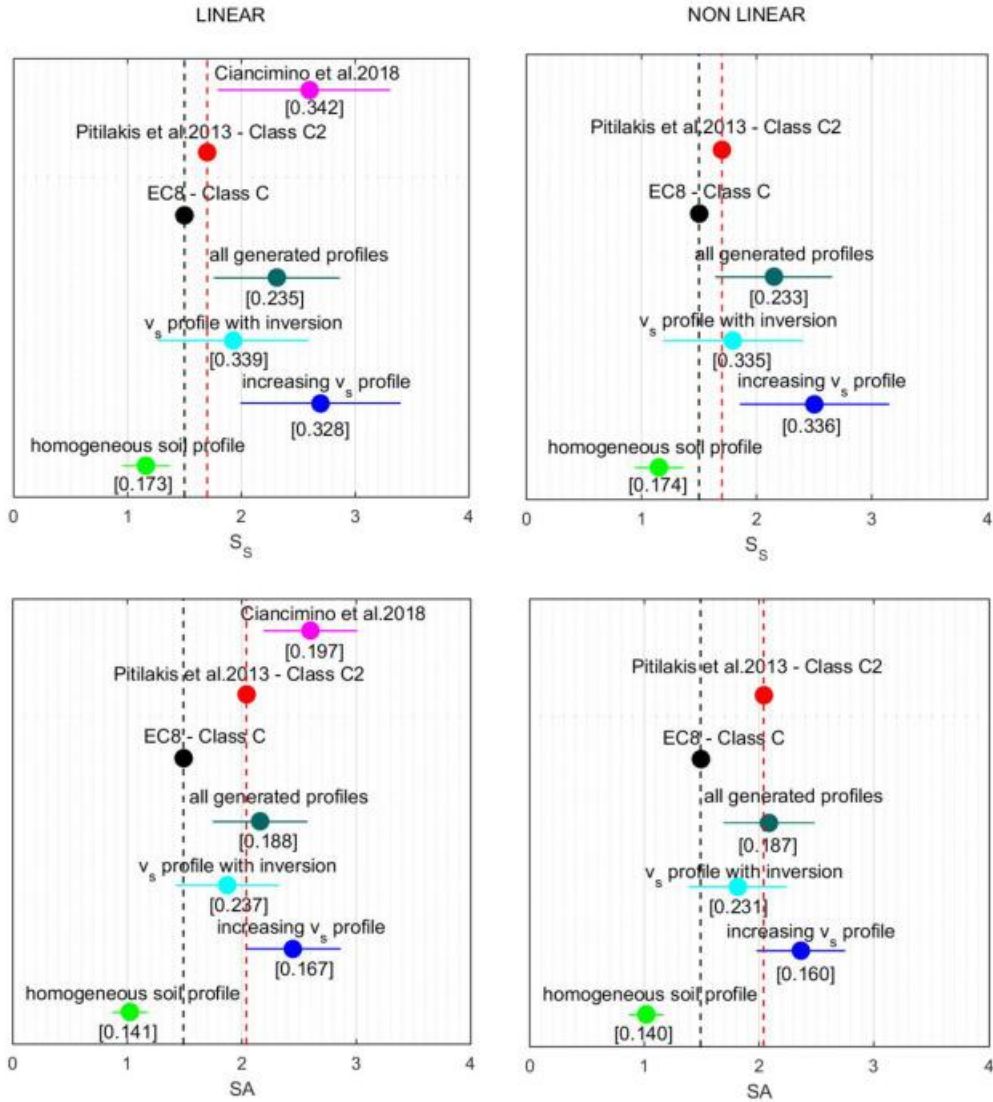
479 It is interesting to note that the values proposed by Pitilakis et al. [18] for the site
480 amplification factor SA are close to those computed using the set of generated samples in the
481 present analysis. Conversely, the values proposed by Pitilakis et al. [18] for the site
482 amplification factor S_s are lower than those obtained in the present research. This means that
483 ground classification based on complementary site proxies instead on a single proxy is more
484 adequate. But also it is important to understand the best complementary proxies that allow
485 predicting the site response for different ranges of periods.

486 Moreover, the nonlinear effects are negligible in terms of mean values and CV of the
487 amplification factors, for weak earthquakes (Fig. 12) and they are significant for strong
488 earthquakes (Fig. 13).

489 The average amplification factors obtained for soil profiles with a velocity inversion are lower
490 than the ones associated to other soil profiles.

491 Lastly, Fig. 14 shows that the comparison between the computed amplification factors and
492 those deduced by New Zealand Standard [26]. The difference observed could be justified by a
493 higher seismicity expected in New Zealand that could increase the effect of nonlinear soil
494 behavior and thus reduce the peak acceleration.

TYPE 2



495

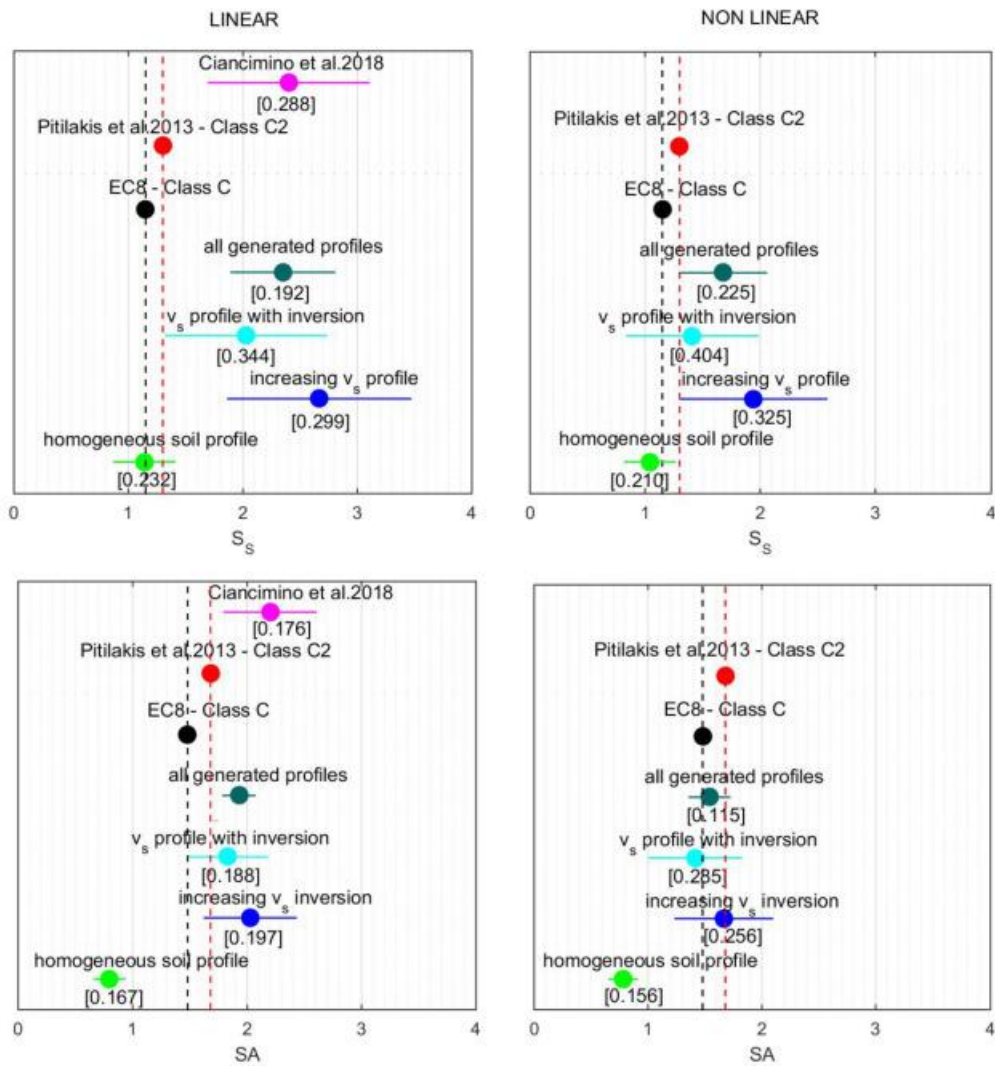
496

(a)

(b)

497 Fig. 12. Mean value of site amplification factors S_s (top) and SA (bottom), the values within
 498 one standard deviation of the mean and the coefficient of variation CV (value between
 499 brackets) in the case of small earthquakes (type 2 response spectrum of Eurocode 8 [25]), for
 500 numerical simulations under the assumption of linear (a) and nonlinear (b) soil behavior. The
 501 values suggested by Eurocode 8 [25], Pitilakis et al. [18] and Ciancimino et al [24] are
 502 indicated.

TYPE 1



(a)

(b)

503

504

505 Fig. 13. Mean value of site amplification factors S_s (top) and SA (bottom), the values within

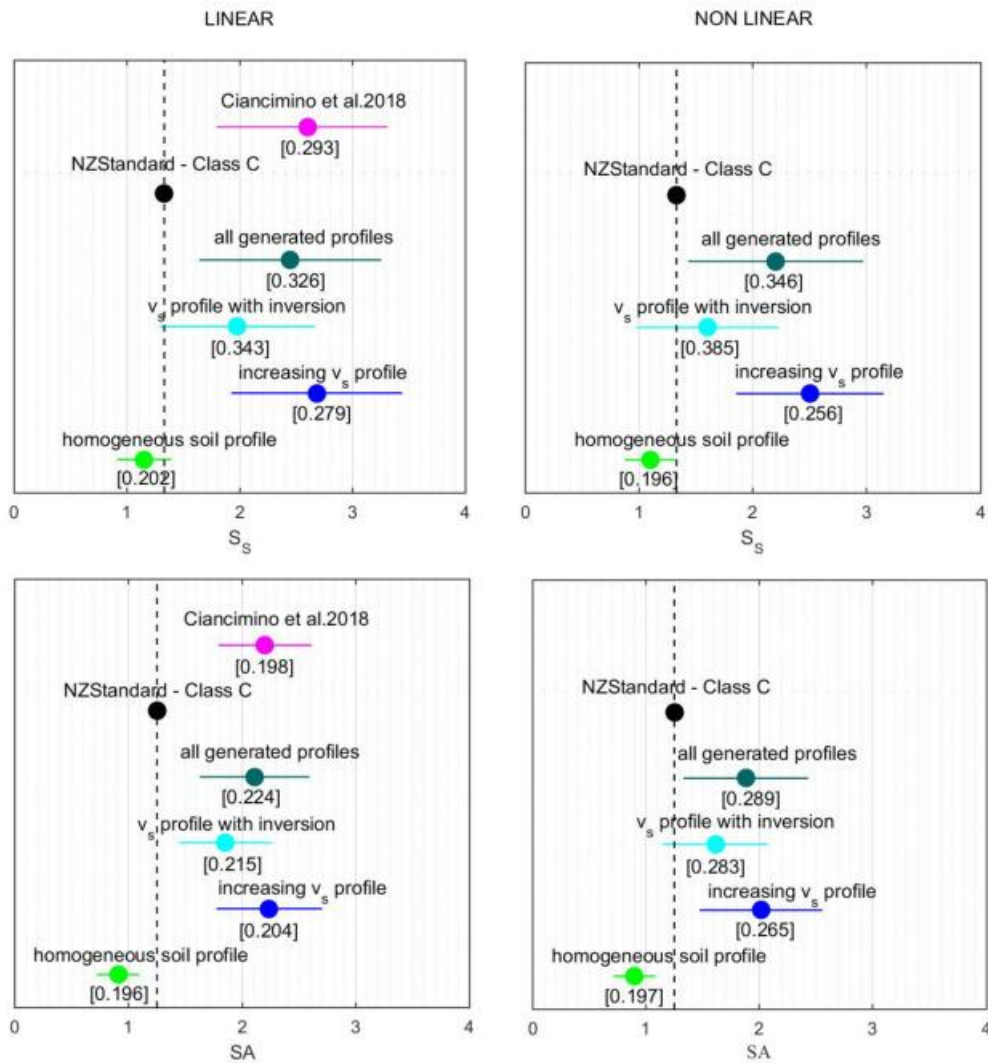
506 one standard deviation of the mean and the coefficient of variation CV (value between

507 brackets) in the case of strong earthquakes (type 1 response spectrum of Eurocode 8 [25]), for

508 numerical simulations under the assumption of linear (a) and nonlinear (b) soil behavior. The

509 values suggested by Eurocode 8 [25], Pitilakis et al. [18] and Ciancimino et al [24] are

510 indicated.



511

512

513 Fig. 14. Mean value of site amplification factors S_s (top) and SA (bottom), the values within

514 one standard deviation of the mean and the coefficient of variation CV (value between

515 brackets) for the whole set of recorded seismic signals. Numerical simulations under the

516 assumption of linear (a) and nonlinear (b) soil behavior are separated. The values suggested

517 by the New Zealand Standard [26] building codes are indicated.

518

519 4. Conclusions

520 The vertical propagation of various recorded seismic signals along stochastically generated

521 soil profiles is numerically simulated to obtain the FF motion, in both cases of linear and

522 nonlinear soil behavior. The average shear wave velocity in the upper 30m of soil profiles
523 $v_{s,30}$ is fixed and corresponds to the ground type C, according to the Eurocode 8. The soil-
524 bedrock interface depth is selected as $H_{800} = 30$ m .

525 This research highlights the influence of the layering uncertainty on the site response. It is
526 demonstrated that the average shear wave velocity $v_{s,30}$ is not able, as single parameter, to
527 characterize the soil profiles in terms of expected amplification level over the whole
528 frequency range.

529 Two site parameters are proposed as proxies, complementary to $v_{s,30}$, such as the dominant
530 frequency of the site f_0 and the shear wave velocity gradient B_{30} . The site response is
531 represented in terms of site amplification factors, deduced using the response spectrum of the
532 FF motion, for the 24000 performed simulations (set of 40 recorded seismic signals applied to
533 300 generated soil profiles, for linear and nonlinear soil behaviors). The influence on site
534 amplification of the shear wave velocity profile, site dominant frequency and shear wave
535 velocity gradient are analyzed independently from H_{800} .

536 The obtained amplification factors are functions of both site conditions and intensity of rock
537 motions and the values could decrease due to soil nonlinearity. The amplification factors
538 increase with decreasing site dominant period T_0 and increasing shear wave velocity gradient
539 B_{30} , when they are evaluated over a large range of vibration periods $[0.05-2.5\text{s}]$.

540 Nevertheless, site amplification appears strongly dependent on the site predominant period
541 T_0 , for short vibration periods of the FF motion and independent from it for long periods.
542 Moreover, site amplification is much more pronounced in soil profiles having T_0 lower than
543 that of the homogeneous profile, for short vibration periods of the FF motion.

544 The largest values of amplification factors are reached for short vibration periods of the FF
545 motion, lower than 0.5s , in soil profiles having a high shear wave velocity gradient B_{30} ,

546 which corresponds to sites with a large impedance contrast in the first 30m or with a steep
547 slope in the shear wave velocity profile.

548 The site response is modified when the nonlinear soil behavior is taken into account in the
549 numerical simulations. The nonlinear soil behavior on the site response induces a reduced
550 amplification effect. Similarly to the case of linear soil behavior, the site amplification is more
551 pronounced in the case of short vibration periods of the FF motion and it is strongly
552 dependent on the proposed site parameters. On the contrary, the site amplification is less
553 pronounced and independent from the proposed site parameters, for vibration periods of the
554 FF motion higher than 1s.

555 Nonlinear effects are negligible for small earthquakes and for vibration periods of strong
556 ground motions longer than 1s. Whereas, they are significant for short- and middle-periods of
557 strong earthquakes. In particular, soil profiles having dominant period T_0 higher than that of
558 the homogeneous profile exhibit significant nonlinear effects. In addition, soil profiles with
559 negative value of B_{30} (i.e. velocity inversion) and profiles with high value of B_{30} lead to
560 pronounced nonlinear site effects.

561 Average amplification factors are compared to those suggested by Eurocode 8 [25] and New
562 Zealand Standard [26] building codes, and by Pitilakis et al. [18]. The obtained results
563 demonstrate that the ground type classification proposed by Eurocode 8 [25], based on $v_{s,30}$
564 only, is not suitable. The comparison to the amplification factors proposed by Pitilakis et al.
565 [18] shows that the introduction of complementary site proxies makes the ground type
566 classification more adequate. In fact, the computed average spectral amplification factors SA
567 are comparable to those estimated by Pitilakis et al. [18].

568 The average amplification factors computed for soil profiles with a velocity inversion are
569 lower than for the profiles having monotonic shear wave velocity profiles.

570 This research confirms that it is possible to improve the current ground type classification

571 taking into account simple and accessible site parameters complementary to $v_{s,30}$. Accounting
572 for complementary site proxies in the ground type classification, such as the dominant
573 frequency of the site f_0 and the shear wave velocity gradient B_{30} , allow a better prediction of
574 the expected amplification, in particular for short vibration periods of the FF motion, up to 1s.
575 Further work should be done to analyze the results for soil profiles having different ground
576 types according to the Eurocode 8 (only ground type C has been discussed in this research)
577 and depth H_{800} .

578

579 **6. References**

- 580 [1] Semblat JF, Kham A, Parara E, Bard P, Pitilakis K, Makra K, et al. Seismic wave
581 amplification : Basin geometry vs soil layering . Soil Dynamics and Earthquake Eng.
582 2005; 25(7-10):529-538. 2009.
- 583 [2] Borchardt RD. Estimates of site-dependent response spectra for design (methodology
584 and justification). Earthq Spectra 1994;10:617–53.
- 585 [3] Dickenson, S. E. and RBS. Nonlinear dynamic response of soft and deep cohesive soil
586 deposits. Proc. Int. Work. site response Subj. to strong Earthq. motions, 1996, p. 67–
587 81.
- 588 [4] Dobry, R., Borchardt, R. D., Crouse, C. B., Idriss, I. M., Joyner, W. B., Martin, G. R.,
589 Seed RB. New site coefficients and site classification system used in recent building
590 seismic code provisions. Earthq Spectra 2000;16:41–67.
- 591 [5] Seyhan, E., Stewart, J. P., Ancheta, T. D., Darragh, R. B., & Graves RW. NGA-West2
592 site database. Earthq Spectra 2014;30:1007–24. doi:10.1193/062913EQS180M.
- 593 [6] Seyhan E, Stewart JP. Semi-Empirical Nonlinear Site Amplification from NGA-West2
594 Data and Simulations. Earthq Spectra 2014;30:1241–56.
595 doi:10.1193/063013EQS181M.

- 596 [7] Derras B, Bard PY, Cotton F. Site-condition proxies, ground motion variability, and
597 data-driven GMPEs: Insights from the NGA-West2 and RESORCE data sets. *Earthq*
598 *Spectra* 2016;32:2027–56. doi:10.1193/060215EQS082M.
- 599 [8] Park D, Hashash YMA. Probabilistic seismic hazard analysis with non linear site
600 effects in the Mississippi embayment. 13 th World Conf. Earthq. Eng., 2004, p. 1549.
- 601 [9] Mucciarelli M, Gallipoli MR. Comparison between Vs30 and other estimates of site
602 amplification in Italy. *First Eur Conf Earthq Eng Seismol* 2006:270.
- 603 [10] Castellaro S, Mulargia F, Rossi PL. Vs30: Proxy for Seismic Amplification? *Seismol*
604 *Res Lett* 2008;79:540–3. doi:10.1785/gssrl.79.4.540.
- 605 [11] Cadet H, Bard PY, Duval AM. a New Proposal for Site Classification Based on
606 Ambient Vibration Measurements and the Kiknet Strong Motion Data Set. 14th World
607 Conf Earthq Eng 2008.
- 608 [12] Luzi L, Puglia R, Pacor F, Gallipoli MR, Bindi D, Mucciarelli M. Proposal for a soil
609 classification based on parameters alternative or complementary to Vs,30. *Bull Earthq*
610 *Eng* 2011;9:1877–98. doi:10.1007/s10518-011-9274-2.
- 611 [13] Cadet H, Bard PY, Duval AM, Bertrand E. Site effect assessment using KiK-net data:
612 Part 2-site amplification prediction equation based on f0 and Vsz. *Bull Earthq Eng*
613 2012;10:451–89. doi:10.1007/s10518-011-9298-7.
- 614 [14] Derras B, Bard PY, Cotton F. VS30, slope, H800 and f0: Performance of various site-
615 condition proxies in reducing ground-motion aleatory variability and predicting
616 nonlinear site response 4. *Seismology. Earth, Planets Sp* 2017;69:0–21.
617 doi:10.1186/s40623-017-0718-z.
- 618 [15] Castelli F, Cavallaro A, Grasso S, Lentini V. Seismic microzoning from synthetic
619 ground motion earthquake scenarios parameters: The case study of the city of Catania
620 (Italy). *Soil Dyn Earthq Eng* 2016;88:307–27. doi:10.1016/j.soildyn.2016.07.010.

- 621 [16] Steidl JH. Site response in southern California for probabilistic seismic hazard analysis.
622 Bull Seismol Soc Am 2000;90:149–69. doi:10.1785/0120000504.
- 623 [17] Kotha, S. R., Cotton, F., & Bindi D. A New Approach to Site Classification : Mixed-
624 effects Ground Motion Prediction Equation with Spectral Clustering of Site
625 Amplification Functions. Soil Dyn Earthq Eng 2018;110:318–29.
- 626 [18] Pitilakis K, Riga E, Anastasiadis A. New code site classification, amplification factors
627 and normalized response spectra based on a worldwide ground-motion database. Bull
628 Earthq Eng 2013;11:925–66. doi:10.1007/s10518-013-9429-4.
- 629 [19] Castellaro S, Mulargia F. Simplified seismic soil classification: The Vfz matrix. Bull
630 Earthq Eng 2014;12:735–54. doi:10.1007/s10518-013-9543-3.
- 631 [20] Zhao JX, Irikura K, Zhang J, Fukushima Y, Somerville PG, Asano A, et al. An
632 empirical site-classification method for strong-motion stations in Japan using H/V
633 response spectral ratio. Bull Seismol Soc Am 2006;96:914–25.
634 doi:10.1785/0120050124.
- 635 [21] Gallipoli MR, Mucciarelli M. Comparison of site classification from VS30, VS10, and
636 HVSR in Italy. Bull Seismol Soc Am 2009;99:340–51. doi:10.1785/0120080083.
- 637 [22] Boudghene Stambouli A, Zendagui D, Bard PY, Derras B. Deriving amplification
638 factors from simple site parameters using generalized regression neural networks:
639 Implications for relevant site proxies. Earth, Planets Sp 2017;69. doi:10.1186/s40623-
640 017-0686-3.
- 641 [23] Zhu C, Pilz M, Cotton F. Which is a better proxy, site period or depth to bedrock, in
642 modelling linear site response in addition to the average shear-wave velocity? Bull
643 Earthq Eng 2019:1–24. doi:10.1007/s10518-019-00738-6.
- 644 [24] Ciancimino A, Foti S, Lanzo G. Stochastic analysis of seismic ground response for site
645 classification methods verification. Soil Dyn Earthq Eng 2018;111:169–83.

- 646 doi:10.1016/j.soildyn.2018.04.006.
- 647 [25] European Committee for Standardization (CEN). Eurocode 8: Design of structures for
648 earthquake resistance—Part 1: General rules, seismic actions and rules for buildings
649 (EN 1998-1: 2004). Eur Comm Norm Brussels 2004.
- 650 [26] 1170.5:2004 NZS. Structural Design Actions - Part 5: Earthquake actions- New
651 Zealand. Struct Des Actions 2004.
- 652 [27] Brûlé S, Javelaud E. H/V method in geotechnical engineering. Application to a two
653 layers model. Rev Fr Geotech 2013;142.
- 654 [28] Régnier J, Cadet H, Bonilla LF, Bertrand E, Semblat JF. Assessing Nonlinear Behavior
655 of Soils in Seismic Site Response : Statistical Analysis on KiK-net Strong-Motion
656 Data. Bull Seismol Soc Am 2013;103:1750–70. doi:10.1785/0120120240.
- 657 [29] Régnier J, Cadet H, Bard PY. Empirical quantification of the impact of nonlinear soil
658 behavior on site response. Bull Seismol Soc Am 2016;106:1710–9.
659 doi:10.1785/0120150199.
- 660 [30] Santisi d’Avila MP, Lenti L, Semblat JF. Modelling strong seismic ground motion:
661 Three-dimensional loading path versus wavefield polarization. Geophys J Int
662 2012;190:1607–24. doi:10.1111/j.1365-246X.2012.05599.x.
- 663 [31] Santisi d’Avila MP, Semblat JF, Lenti L. Strong ground motion in the 2011 Tohoku
664 earthquake: A one-directional three-component modeling. Bull Seismol Soc Am
665 2013;103:1394–410. doi:10.1785/0120120208.
- 666 [32] Yokota K, Imai T, Konno M. Dynamic deformation characteristics of soils 1981:13–
667 37.
- 668 [33] Darendeli MB. Development of a new family of normalized modulus reduction and
669 material damping curves. PhD thesis, The University of Texas at Austin, 2001.
- 670 [34] Massa M, Pacor F, Luzi L, Bindi D, Milana G, Sabetta F, et al. The Italian

- 671 ACcelerometric Archive (ITACA): Processing of strong-motion data. *Bull Earthq Eng*
672 2010. doi:10.1007/s10518-009-9152-3.
- 673 [35] Ambraseys NN, Smit P, Douglas J, Margaris B, Sigbjörnsson R, Ólafsson S, et al.
674 Internet site for European strong-motion data. *Boll Di Geofis Teor Ed Appl*
675 2004;45:113–29.
- 676 [36] PEER PEERC. PEER Ground Motion Database. *Shallow Crustal Earthquakes Act*
677 *Tecton Regimes, NGA-West2 2013.*
- 678 [37] Cameron WI, Green RA. Soil Nonlinearity versus Frequency Effects. *Int Work*
679 *Uncertainties Nonlinear Soil Prop Their Impact Model Dyn Response 2004:1–7.*
- 680 [38] Newmark NM, Hall WJ. *Earthquake Spectra and Design, Earthquake Engineering*
681 *Research Center. Berkeley, CA 1982:103.*
- 682 [39] Kawase H. Strong motion characteristics and their damage impact to structures during
683 the off pacific coast of tohoku earthquake of march 11, 2011: How extraordinary was
684 this M 9. 0 earthquake. *4th IASPEI/IAEE Int. Symp., 2011.*
- 685 [40] Régnier J, Bonilla LF, Bard PY, Bertrand E, Hollender F, Kawase H, et al.
686 International benchmark on numerical simulations for 1D, nonlinear site response
687 (Prenolin): Verification phase based on canonical cases. *Bull Seismol Soc Am*
688 2016;106:2112–35. doi:10.1785/0120150284.
- 689 [41] Régnier J, Bonilla LF, Bard PY, Bertrand E, Hollender F, Kawase H, et al. Prenolin:
690 International benchmark on 1D nonlinear: Site-response analysis—validation phase
691 exercise. *Bull Seismol Soc Am* 2018;108. doi:10.1785/0120170210.
- 692 [42] Joyner WB, Chen ATF. Calculation of nonlinear ground response in earthquakes. *Bull*
693 *Seismol Soc Am* 1975;65:1315–36.
- 694 [43] Iwan W.D. On a class of models for the yielding behavior of continuous and composite
695 systems. *J Appl Mech* 1967;34:612–7.

- 696 [44] Joyner WB. A method for calculating nonlinear seismic response in two dimensions.
697 Bull Seismol Soc Am 1975;65:1337–57.
- 698 [45] Régnier J, Bonilla LF, Bertrand E, Semblat JF. Influence of the VS profiles beyond 30
699 m depth on linear site effects: Assessment from the KiK-net Data. Bull Seismol Soc
700 Am 2014;104:2337–48. doi:10.1785/0120140018.
- 701 [46] Rey J, Faccioli E, Bommer JJ. Derivation of design soil coefficients (S) and response
702 spectral shapes for Eurocode 8 using the European Strong-Motion Database. J Seismol
703 2002;6:547–55. doi:10.1023/A:1021169715992.
- 704 [47] Housner GW. Spectrum Intensities of Strong-Motion Earthquakes. Symp Earthq Blast
705 Eff Struct 1952:20–36.
- 706 [48] Kramer S. Geotechnical Earthquake Engineering. Prentice H. Upper Saddle River:
707 1996.
708